Smoke Removal and Image Enhancement of Laparoscopic Images by An Artificial Multi-Exposure Image Fusion Method

Muhammad Adeel Azam
University of Genoa: Universita degli Studi di Genova
Khan Bahadar Khan (kb.khattak@gmail.com)
Islamia University of Bahawalpur https://orcid.org/0000-0003-1409-7571
Eid Rehman
Foundation University Islamabad
Sana Ullah Khan
KUST: Kohat University of Science and Technology

Research Article

Keywords: Artificial multi-exposure fusion, Smoke removal, Laparoscopic Images, Image fusion and enhancement

Posted Date: October 26th, 2021

DOI: https://doi.org/10.21203/rs.3.rs-975713/v1

Version of Record: A version of this preprint was published at Soft Computing on April 11th, 2022. See the published version at https://doi.org/10.1007/s00500-022-06990-4.

Type of the Paper (Article)

Smoke Removal and Image Enhancement of Laparoscopic Images by an Artificial Multi-Exposure Image Fusion Method

Muhammad Adeel Azam [1], Khan Bahadar Khan [2,*], Eid Rehman[3] and Sana Ullah Khan[4]

[1] Department of Advanced Robotics, Istituto Italiano di Tecnologia, Via S. Quirico, 19d, 16163 Genova, Italy; adeel.azam@iit.it ,
[1] Department of Informatics, Bioengineering, Robotics, and System Engineering, University of Genoa, Genoa, Italy; adeel.azam@iit.it
[2] Department of Telecommunication Engineering, Faculty of Engineering, The Islamia University of Bahawalpur, 63100, Pakistan; kb.khattak@gmail.com
[3] Department of Software Engineering, Foundation University, Rawalpindi Campus, Pakistan; eidrehmanktk@fui.edu.pk
[4] Institute Institute of Computing, Kohat University of Science and technology Kohat (KUST), KPK, Pakistan. sana.ullah@kust.edu.pk
* Correspondence: kb.khattak@gmail.com ;

Abstract: In laparoscopic surgery, image quality is often degraded by surgical smoke or by side effects of the illumination system, such as reflections, specularities, and non-uniform illumination. The degraded images complicate the work of the surgeons and may lead to errors in image-guided surgery. Existing enhancement algorithms mainly focus on enhancing global image contrast, overlooking local contrast. Here, we propose a new Patch Adaptive Structure Decomposition utilizing the Multi-Exposure Fusion (PASD-MEF) technique to enhance the local contrast of laparoscopic images for better visualization. The set of under-exposure level images are obtained from a single input blurred image by using gamma correction. Spatial linear saturation is applied to enhance image contrast and to adjust the image saturation. The Multi-Exposure Fusion (MEF) is used on a series of multi-exposure images to obtain a single clear and smoke-free fused image. MEF is applied by using adaptive structure decomposition on all image patches. Image entropy based on the texture energy is used to calculate image energy strength. The texture entropy energy determined the patch size that is useful in the decomposition of image structure. The proposed method effectively eliminate smoke and enhance the degraded laparoscopic images. The qualitative results showed that the visual quality of the resultant images is improved and smoke-free. Furthermore, the quantitative scores computed of the metrics: FADE, Blur, JNBM, and Edge Intensity are significantly improved as compared to other existing methods.

Keywords: Artificial multi-exposure fusion; Smoke removal; Laparoscopic Images; Image fusion and enhancement;

1. Introduction

Laparoscopic imaging modalities play a significant role in navigation during operation and treatment planning. Medical surgeons always focus on the quality of images that determine the best medical decision for the operating environment [1]. In laparoscopic surgery, a small size camera is injected into the human body through a small incision. All the internal body structural and functional information can be seen and monitored with the help of an LCD screen placed in the operation room [2]. The CO2 gas is inserted into the human abdominal area to expand the internal space so that surgical instruments can be easily operated on. The CO2 gas and dissection deformation of tissues produce smoke that causes the invisibility of organs [3]. The degradation and artifacts in laparoscopic images produce also due to many other factors such as dynamic homogenous internal structure, blood flow, dynamic illumination factor, optical instruments reflection, etc. [4]. The

https://doi.org/10.3390/xxxxx

smoke effect during laparoscopic can severely degrade the image quality and also its effects on radiance information of image patches. The degraded and blurred images could reduce the visibility of the surgeon for diagnosis and also increase the probability of error during surgery. The smoke removal could reduce not only the surgery time but also important for surgery planning and treatment. Therefore, an accurate smoke removal algorithm is required for better visualization of laparoscopic images [3-5].

There are many clinical applications of laparoscopy images and it can help to diagnose multiple diseases at a very early stage. The smoke removal method is considered as image de-hazing that existed in literature [6-7]. The image de-hazing algorithms are classified into two groups: image restoration and image enhancement [8-9]. In the image restoration category, the haze-free image is obtained by using atmospheric degradation methods utilizing prior knowledge of image depth information. The prior information of hazy image derived first then by applying physical degradation model to obtain haze-free images. He et al. [8] proposed Dark Channel Prior (DCP) technique that is based on the restoration domain. While in the image enhancement domain, there is no need of using an atmospheric physical model and prior estimation of depth information in images. In this method, the correlation algorithms are mostly used to enhance the local contrast of the images for better visualization [10]. In this category, some of the techniques are the Retinex algorithm [12], fusion-based [13], Histogram equalization [12-13], and wavelet-based algorithms [16]. In fusion-based methods, the resultant enhanced image is obtained by fusing input blurred images. However, the required detailed information at a high level of accuracy in smoke-free images is still a challenging task. Gamma correction is utilized to split single input blurry and smoky images into different multi-exposure images then the MEF technique is implemented to fuse these multi-exposure images. The image contrast and saturation are used as image fusion weights during the fusion process. MEF techniques are used for enhancing the visual quality of degraded images [17]. In the enhancement domain, existing smoke removal algorithms are used to enhance the saturation and global contrast of images while neglecting the local contrast information. Image visual quality is affected due to the missing of many local pixels during the calculation of global contrast.

In this article, we proposed a laparoscopic smoke removal method that removes the smoke effect and also enhanced the quality of the degraded images. The proposed method is based on the PASD-MEF technique. The MEF technique enhanced the local detail information of input laparoscopic images. A series of gamma correction is used to remove the blurry patches in the images and also effectively increase the local contrast of the images. Whereas, the Spatial Linear Saturation (SLS) is used to increase the color saturation of the laparoscopic images. Then, a set of images with under-exposure levels are formed. These under-exposure images now have high color saturation and enhanced contrast but low exposure levels. The proposed algorithm implemented a patch adaptive structure (PAS) technique that works on MEF. The advantage of using PAS and MEF is that it preserved the structure of laparoscopic images. The significant contribution of the proposed methodology is highlighted as follows:

- Development of smoke removal self-fusion algorithm on smoky and blurry input images in a spatial domain. The smoke effect is removed with the help of contrast and saturation correction. SLS is implemented to increase the saturation contrast of images.
- PASD algorithm is proposed for the spatial domain, MEF to enhance the visual quality of the degraded blur laparoscopic images. The adaptive selection of different patched size in images are obtained by using an implementation of block size and texture energy. Adaptive selection avoids the error of loss of information in both local structure and texture detail information of images during the smoke removal procedure.
- The proposed algorithm PASD-MEF is verified both in a qualitative as well as quantitative manner. The article demonstrated that the proposed algorithm not only removes the smoke but also enhances the visual quality of the laparoscopic image for better visualization and diagnostic purposes.

- The proposed algorithm is compared with other state-of-the-art smoke removal methods and the proposed method showed significantly improved performance in terms of visual and statistical evaluation metrics.

The article arrangement is as follows: In Sec. 2, related works associated with haze and de-smoke is presented while Sec. 3 describes the proposed methodology. In Sec. 4, the quantitative and qualitative results are encapsulated and the conclusion is drawn in Sec. 5.

2. Related Works

There are many techniques presented in the literature for de-smoke of laparoscopic image [3-5]. A novel Bayesian inference that consists of a probabilistic graphical technique is applied on laparoscopic images [3]. The model includes a prior model and is implemented on transmission map images. The transmission map is useful for color attenuation that is caused by smoke. Then, this work is extended in [4], to achieve smoke-free, noiseless, and remove the specular effect in images. There are many other methods in the literature that are related to laparoscopic smoke removal. These techniques use the atmospheric scattering model and work relatively the same as the dehazing techniques in the literature. The atmospheric model depends on the depth of images or the transmission map [6], [16-17]. He at el. proposed a DCP technique that relies on statistical observation and implemented on outdoor hazy images [6], [16-17]. In this method, it is observed that mostly pixels having very low intensities values in at minimum single-color channel. In the DCP method, a prior estimation knowledge of image depth detail and transmission map is implemented. The density of the hazing scene acquired and high-quality non-hazy images are formed. This algorithm not effectively works on outdoor images that have a very high white radiance effect. However, some other methods do not require estimation of transmission map or image depth information. Tan et al. [9] directly enhance the local detail of images without any use of a transmission map. In [13], a fusion-based method is proposed that relies on white balance phenomena to enhance the input images. A Laplacian pyramid representation technique is used for fusion purposes and this method works on per-pixel. The multi-scale fusion is implemented on hazy images and derived single resultant image. Most of the image smoke removal methods work as image restoration and on smoke removal. Koschmieder [20] proposed an atmospheric scattering scheme to solve the problem of degradation in images caused by smoke. This model is described in Eq.1.

$$I\ (y) = \ t\ (y).J\ (y) + \ A.(1 - t\ (y)) \tag{1}$$

Where I(y) represent the degraded images while J(y) is the haze-free image. The t(y) denotes the transmission medium and represents the quantity of light that spreads toward the target. In the above equation, the A denotes global atmospheric light. The product of t (y).J (y) represents the scene radiance. The term $A.\left(1 - t\ (y)\right)$ in Eq. 1 denote the air-light. Air light produced by smoke dispersion increases the intensity of the object, which is assumed to be the primary cause of the color shift of the scene. This term for air light, especially for thick smoke, would dominate the strength of the scene. By rearranging the above equation the haze-free image J(y) will be achieved. The haze-free image only is obtained when the value of A and t(y) are already achieved using apriori information and from the estimation solution. Eq.2 represents the rearranged form of equation (1). The common limitation J (x) can also be limited by implementing the maximum local contrast and saturation or distributing the specific color pixels in RGB space.

$$J(y) = \ \frac{I(y) - A}{t\ (y)} + \ A \tag{2}$$

In this paper, we proposed a multi-exposure image fusion method for smoke removal, adjustment of saturation, and contrast of images. The Multi-exposure fusion techniques are also used in many image processing tasks where different sensors sequence of images fused to obtained resultant single image [15], [19-20]. The existence of image fusion methods discussed in the literature are based on sparse representation [21-23], guided filtering techniques [26], Multi-scale decomposition fusion techniques [25-27], patch structure decomposition [30], and multi-exposure image fusion. However, MEF methods are not only used for image smoke removal but also image enhancement [10, 31]. Galdran introduced multi-exposure fusion based on Laplacian pyramid fusion (LPF) for haze removal [10], then, in the space domain, the haze removal is converted to increase image contrast and saturation effect. The LPF weight is used to manipulate image contrast and saturation that enhance the visual quality of images. The gamma correction and image enhancement work in spatial domain, the gamma correction method is widely used in literature for image enhancement [10]. Histogram Equalization is added to gamma correction to increase the image contrast. Whereas traditional image enhancement methods are used for global contrast and saturation transformation of images. In the proposed methodology, the Adaptive Gamma Correction (AGC) technique is used to increase the transmission map t(x) that is used in Equation (1) by the Koschmieder model. For further improvement of AGC, we used Laplacian based solutions. Contrast adjustment solution integrated with AGC to remove the blurred effect in images.

3. Proposed Methodology

To avoid the estimation effect of atmospheric light and transmittance described in Equation (1), the contrast enhancement and saturation adjustment technique in the spatial domain is suggested to achieve smoke-free laparoscopic images. According to Koschmieder model the intensity range of input blurred images I(y) lies between values 0 to 1. The following condition $J(y) \leq I(y)\ \forall\ y$ needs to satisfy to obtain smoke-free image J(y). In this paper, we first make a set of under-exposed images U= {I1(y), I2(y), I3(y)…...Ik(y)} from the original smoke input image I(y). The under-exposed images always reduce the intensity variation in images. The under-exposure image I(y) inset of multiple under-exposure images contain high contrast and saturation but skip small detail structure information. These under-exposure images now have low exposure levels. We implemented a MEF technique to fuse all the under-exposed set of images U= {I1(y), I2(y), I3(y)…...Ik(y)} into a single image to extract local detail information. The MEF technique fused different regions of images with good contrast and saturation level to obtain smoke-free single image J(y). The flowchart of the proposed methodology is shown in Fig.1. First, the set of multi-exposure images are obtained with the help of gamma correction. The linear adjustment associated with spatial saturation is also implemented on the image to increase the visual quality. Gamma correction is implemented for contrast level adjustment of images. The increase of the contrast of blurred areas in the images decreased the sharpness level of that area. To overcome this problem, we utilized a MEF technique that extracts those corresponding areas from multiple images and fused them into a single image with better contrast and saturation. For better fusion, it is important to maintain texture and color detail as same as the original image which is achieved by applying MEF with adaptive structure decomposition (ASD) of the image patch. In the proposed methodology, the texture information components of the image are obtained by using cartoon texture decomposition [32]. The image texture entropy is calculated from the gray difference technique. The texture entropy value and image block size are treated in an image decomposition block. The overall image block is sub-divided into three independent components. Each component process individually to give the resultant fused smoke-free image. The proposed methodology is explained in the following sections.

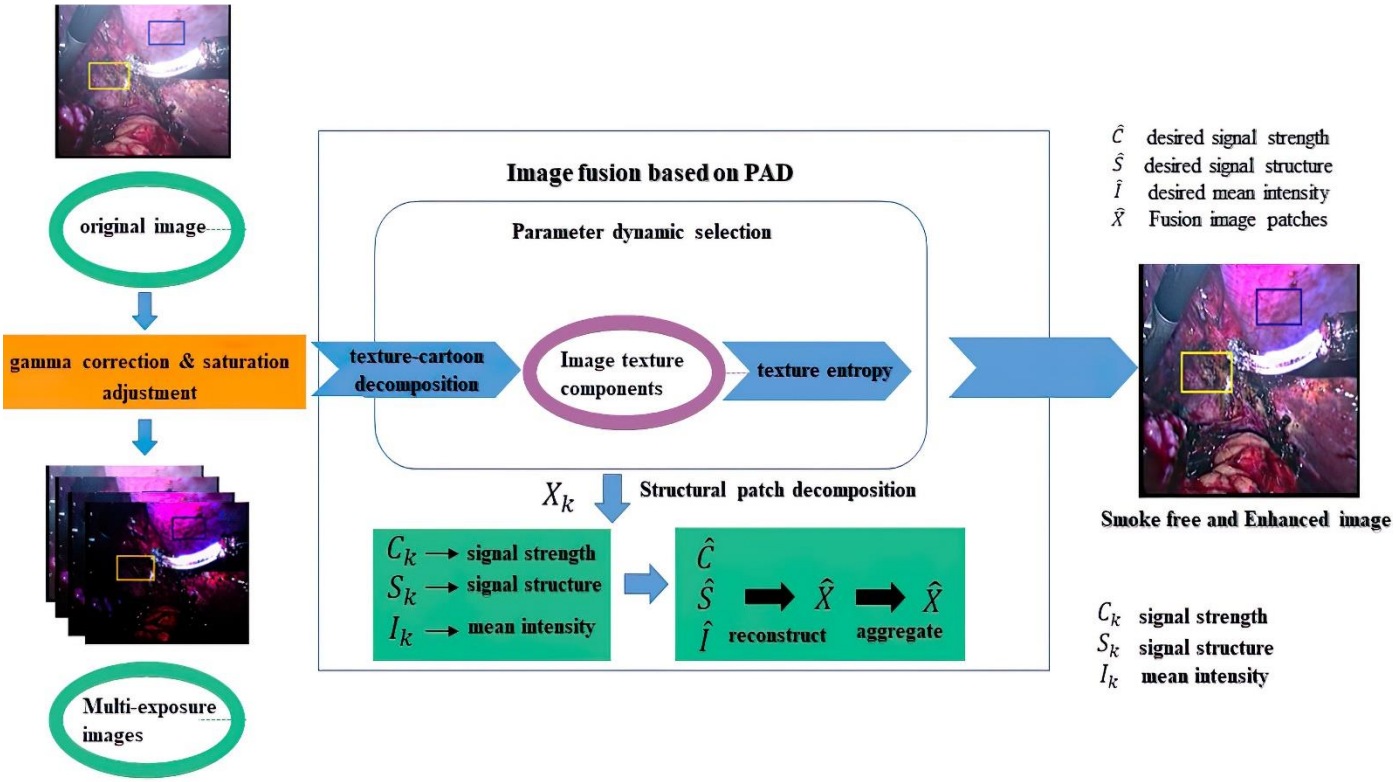

Figure 1. Proposed methodology PASD-MEF framework.

3.1. Gamma Correction and Contrast Adjustment

The overall image intensity of degraded image I(y) is adjusted by using gamma correction and modify the intensity of the image by a power function as shown in Equation (3).

$$I(y) \rightarrow \beta . I(y)^{\mu} \quad (3)$$

Where the term β and μ represent the positive constant. The visual differences are more prominent in the dark areas as compared to bright areas. The value of μ has chosen less than one μ < 1 for compressed bright intensities while it increases dark intensities in images for better visual detail. The value of μ > 1, more bright intensities are allotted in a more extensive range after transformation, and dark intensities are compressed for that value range. The contrast of the image region can be expressed in Equation (4).

$$C(\omega) = I^{\omega}_{max} - I^{\omega}_{min} \quad (4)$$

Where I^{ω}_{max}= max {I(y) | y ϵ ω} and I^{ω}_{min}= min {I(y) | y ϵ ω}. In Fig. 3(e) and 4(e), the image shows overexposure and there is contrast detail information missing in both images. After applying the μ > 1 operation, the contrast detail of the image in Fig. 3(g) and 4(g) increases. In our proposed algorithm, the adjustment of gamma correction is used to modify the local contrast detail of input images. Gamma correction also removes the blurred effect in images as shown in Fig. 2(h) and 3(h). In Figs. 2-3, different exposure level laparoscopic images are shown. The left side images are over-exposure images while the move toward the right side the exposure level of images decreases. The resultant fused MEF images are shown on the rightmost side of Figs. 2-3.

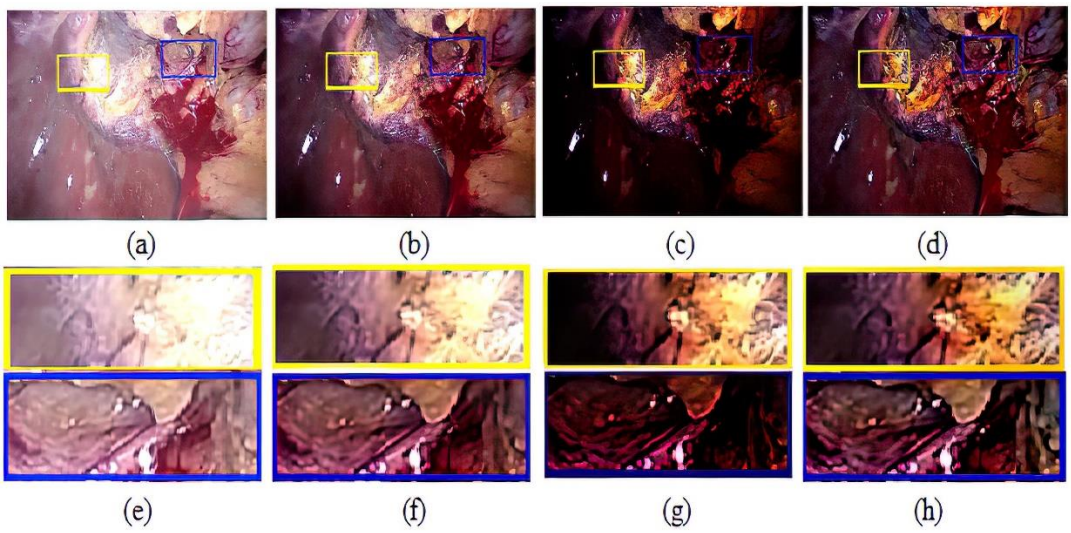

Figure 2. Multi-exposure laparoscopic images of video 1 with smoke Level 3. (a) Over-exposed (b) Normal exposed image (c) under-exposed image (d) Resultant fused image obtained from images (a)-(c). (e) Zoom-in over-exposed image (f) Zoom-in of normally exposed image (g) Zoom-in under-exposed (h) Zoom-in of the fused image.

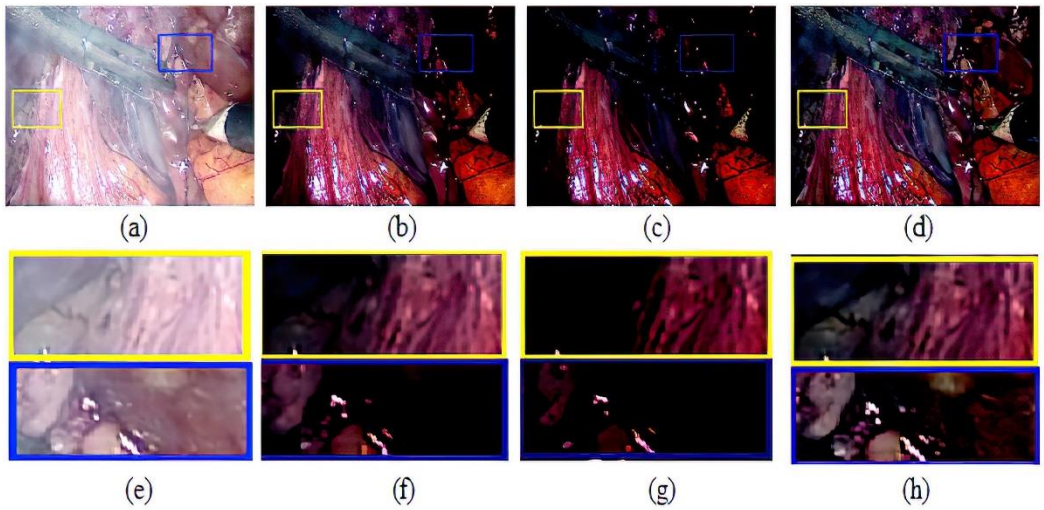

Figure 3. Multi-exposure laparoscopic images of video 10 with smoke Level 4. (a) Over-exposed (b) Normal exposed image (c) under-exposed image (d) Resultant fused image obtained from images (a)-(c). (e) Zoom-in over-exposed image (f) Zoom-in of normally exposed image (g) Zoom-in under-exposed (h) Zoom-in of the fused image.

3.2. Artificial Multi-Exposure Fusion

After the contrast enhancement, the Spatial Linear Saturation (SLS) is implemented on multi-exposure laparoscopic images. The visual quality of images is improved by using the adjustment of local contrast and brightness of the images. The sequence of multi-exposure images U= {I1(y), I2(y), I3(y)…... Ik(y)} from input image I(y) is obtained with the help of gamma correction. For every image $U_k^R(y), U_k^G(y), U_k^B(y)\}$ in the set of multi-exposure the minimum and maximum components value of three-channel R, G, and B can be manipulated by using Equation (5) and (6). When Δ = (RGBmax − RGBmin)/255 > 0, then saturation of every pixel can be manipulated by using Equation (7).

$$\text{RGBmax} = \max(\max(\text{R}, \text{G}), \text{B}) \quad (5)$$

$$\text{RGBmin} = \min(\min(\text{R}, \text{G}), \text{B}) \quad (6)$$

$$S = \begin{cases} \dfrac{\Delta}{value} & L < 0.5 \\ \dfrac{\Delta}{2 - value} & L \geq 0.5 \end{cases} \quad (7)$$

The term value and L can be defined in Equation (8). When the saturation of every pixel value is computed then this operation is applied on each channel of image RGB described as in Equation (9). We have taken the adjustment range of saturation for an image as [0,100].

$$value = \frac{RGBmax + RGBmin}{255}, \qquad Where \qquad L = value/2 \quad (8)$$

$$U_K'(y) = U_k(y) + (U_k(y) - L * 255) * \beta \quad (9)$$

$$\beta = \begin{cases} \dfrac{1}{(S-1)} & percent + S \geq 1 \\ \dfrac{1}{(-percent)} & else \end{cases} \quad (10)$$

The final image obtained after the saturation operation applied on each channel of the image is described in Equation (11).

$$U_K'(y) = (U_k^{R'}(y), U_k^{G'}(y), U_k^{B'}(y)) \quad (11)$$

When the image saturation process is completed then MEF is applied to obtain the local detail information of the laparoscopic images. The proposed MEF scheme works on adaptive decomposition based on patch structure. The adaptive patch of an image determines using image texture entropy and patch size. The resultant fuse image is obtained by combining decompose patch images. The image cartoon decomposition is used for the analysis of structural information in an image [21] while texture components of the image give detailed information [25]. In the proposed work, the Vese Osher (VO) model is implemented based on variational image decomposition [25] [33] to the source images. The cartoon-texture decomposition determines by using Vese Osher (VO) model.

3.3. Adaptive Patch Structure and Image Intensity

When the texture component is determined, the gray difference technique is implemented to compute the image entropy value using texture features. Then adaptive path size selection of the image is selected. If pixel point is located at point (x, y) then a point $p = (\Delta x, \Delta y)$ far away from pixel point is represented as$(x + \Delta x,\ y + \ \Delta y)$. The gray scale based on different value can be calculated as in Equation (12).

$$m_\Delta(x, y) = m(x, y) - m(x + \Delta x, y + \ \Delta y) \quad (12)$$

Where m(x, y) denoted gray scale value and $m_\Delta(x, y)$ represent the difference in gray scale value. The entropy value of laparoscopic images can be determined by using Equation (13).

$$E = \sum_{i=0}^{n} p(i) log_2[p(i)] \quad (13)$$

For complete image texture, the values of entropies can be calculated in the form of set E= {E1, E2, E3……., Ek,}, where E1, E2…... Ek is the entropy value of each image. Then

final entropy value can be calculated by using the mean of all entropy values represented in Equation (14).

$$E = \frac{1}{K} \sum_{i=0}^{k} E_i \tag{14}$$

The adaptive patch size scheme preserved more detailed information during the fusion process. The optimal block size of each image can be calculated by using Equation (15).

$$W_s = P_s \ (0.1) \ x \left(\frac{\left(\frac{E}{10}\right)^{E} - \left(-\frac{E}{10}\right)^{-E}}{\left(\frac{E}{10}\right)^{E} + \left(-\frac{E}{10}\right)^{-E}} \right) + P_s \ (e^{-E} \ x \ (0.1) \tag{15}$$

And, W_s is image patch size. The optimal block size can be achieved using the image entropy value. E in the above equation represents the Entropy value of a given image, these parameters are set for calculated image patch size. When the optimal value of W_s achieved then set of multi-exposure images decompose into sub-image of Ws x Ws size blocks. Structure decomposition algorithm [17] is implemented on each patch size of the image that further divided into the following components: I) Ck, signal contrast strength II) signal structure strength Sk and III) mean intensity Ik. These three parameters have proceeded further to achieve the desired fused image patches $\widehat{X}$. To obtain an appropriate fused patch image we need three desired parameters that are $\widehat{C_k}, \widehat{S_k}, \widehat{I}$, these parameters are explain below;

$\widehat{C_k}$ = The desired contrast strength in the fused image was obtained by merging the highest contrast of all source sets of image patches with the same spatial position.

$\widehat{S_k}$ = The desired signal structure fused block can be calculated by assigning weighted average value to image block contrast using input structure vector.

$\widehat{I_k}$ = To obtained mean intensity components, the global and local mean intensity of the current source image is used as an input.

When $\widehat{C_k}, S_k, \widehat{I_k}$ components are calculated then fused image patch $\hat{X}$ obtained and new vector can be represented as shown in Eq. 16. The proposed MEF gives smoke-free, well exposed, and high contrast images by artificially under-exposed/over-exposed images. The smoke in the image represented in Equation (1) always reduces the intensity level of the images. The proposed algorithm works only on under-exposed images. Furthermore, if the exposure value increased then gamma correction can adjust the contrast of images and increase the visual quality of blurred laparoscopic images.

$$\hat{X} = \widehat{C_k} \ . S_k + \widehat{I_k} \tag{16}$$

Multiple image patches of a fused image can be obtained by sliding the window, the pixels in covering patches are found the average value to give output. At that point, the fused image is formed by using Eq.17.

$$J(x) = \sum_{i=1}^{n} \hat{x}_i \tag{17}$$

4. Experimental Results

In this section, the dataset details and the proposed methodology subjective/qualitative and objective/quantitative results compared with other state-of-the-art techniques such as Dark Channel Prior (DCP) [8], Multilayer Perceptron Method (MPM) [34], Color Attenuation Prior (CAP) [19] is presented. The proposed method is implemented on

MATLAB 2018a software where the hardware specification is Intel® Core i3-4010U CPU of clock speed 1.7GHz and RAM is 4GB.

4.1. Dataset

The dataset taken is a part of the ICIP LVQ Challenge dataset. That is a collection of a total of 800 distorted videos created using a set of 20 reference videos, each 10 seconds long [35], [36]. Obtain these videos from the Cholec80 dataset (http://camma.u-strasbg.fr/datasets). The whole dataset consists of ten category videos group such that smoke videos, blurry, white Gaussian noise videos, etc. All videos with a 16:9 aspect ratio have a resolution 512 by 288 and 25 fps frame rate. We collected videos from the smoke group comprising 80 videos arising from applying SMOKE as distortion to each reference video at 4 different stages. Then each video frame is extracted from 25 different smoke videos as shown in Fig. 4. The resolution of images to test the proposed algorithm is 512 by 288.

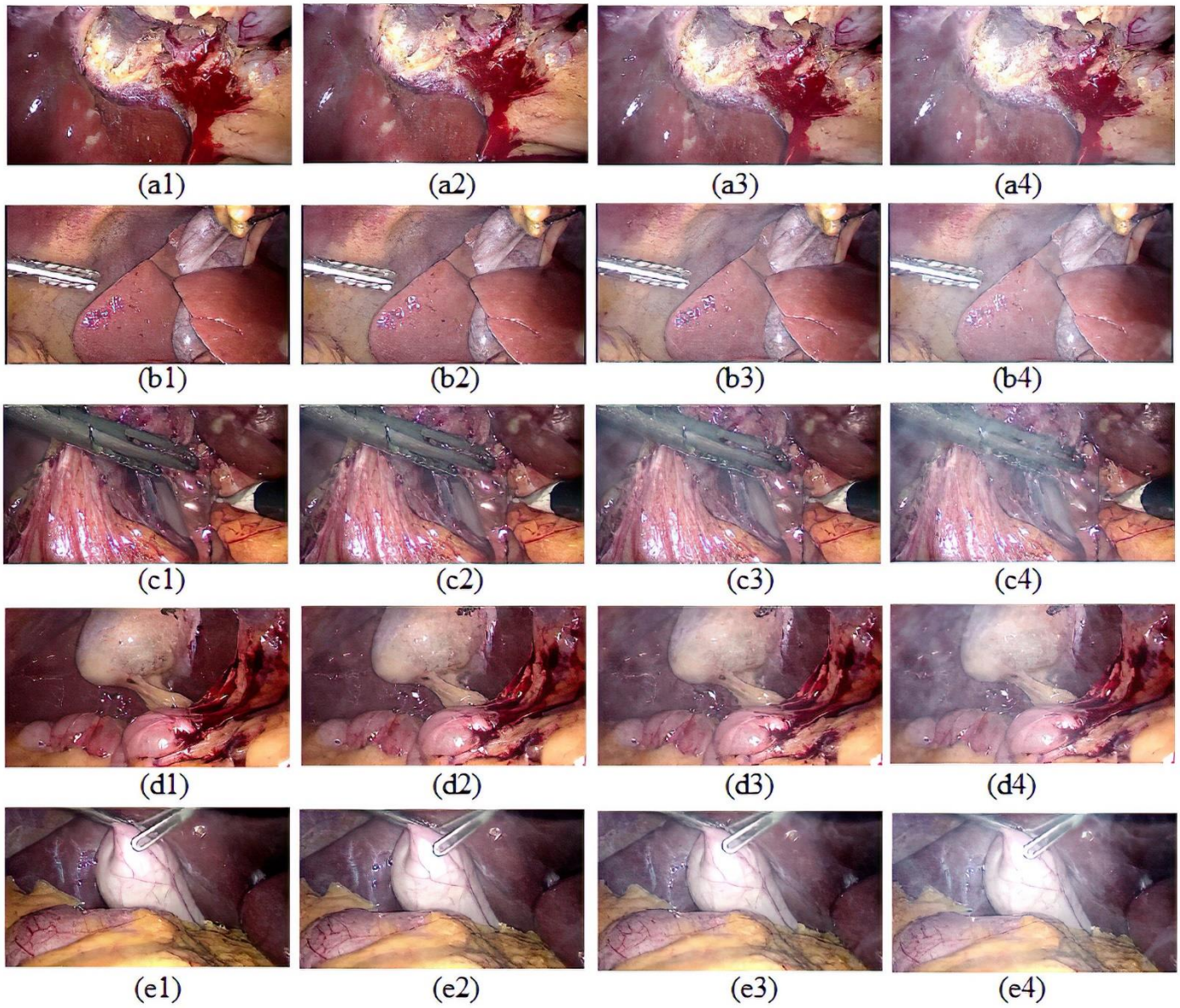

Figure 4. Sample dataset videos frames (a1~a4) frames of video 1 where a1 represent level1 smoke and smoke increase from left to right a4 represent dense smoke of level 4 (b1~b4) frames of video 5 (c1~c4) frames of video 10 (d1~d4) frames extracted from video 15 while (e1~e4) frames of video 20.

4.1.1. Qualitative visual results

The visual results of smoke images with level 3 smoke distortion are shown in Fig. 5 while the smoke images with level 4 distortion are shown in Fig. 6. It is observed that the DCP method can remove the smoke effect but the contrast and saturation balance of images reduces. In the CAP method, it is noticed that smoke is not well removed, and an unbalance natural color of images is also seen. While the MPM method, removes the smoke but local detail information of laparoscopic images is not visible. The proposed method not only removes the smoke from images but also enhanced the local contrast information of the images and the good saturation color are seen.

4.1.1. Quantitative Evaluation

In objective evaluation, we choose non-reference image quality metrics because reference or any ground truth images are absent. The evaluation of the proposed method is performed by computing four metrics: FADE, JNBM, Blur, and Edge intensity. Fog Aware Density Evaluator (FADE) metric is used for analyzing smoke in the images [37-38]. The perceptual fog density in the laparoscopic images can be computed by computing the FADE metric. If the value of FADE is lower, then it means that fog density is lower, for better smoke removal its value should be lower. The JNBM non-reference metric is based on sharpness and works best for blurry images [39-40]. This metric evaluates the quantity level of visual sharpness in the images. The higher value indicated that images are highly sharp and best for perceptual view. Furthermore, an Edge intensity metric is implemented, this metric gives information about the edge intensities that are not visible in source images. The higher value represented good edge intensity [41]. The non-reference blur perceptual metric is used to analyze blurriness in the image. Crete et al. [42] proposed this metric for the first time in image processing. Tab. 1 shows all the statistical results computed by these four non-reference metrics. The proposed method shows a significantly improved result as compared to other state of art techniques. The bold values indicated better performance results. The graphical objective evaluation results of smoke level 3 and level 4 images are shown in Figs. 5-6. The bar-plot result of FADE, JNBM, Blur, and Edge intensity metrics is shown in Figs.7-8.

Table 1. Quantitative/objective evaluation results of the smoke-free images.

Video ID	Smoke frame	Method	FADE	Blur	JNBM	Edge Intensity
1	Level-3	DCP	0.334	0.257	3.3802	69.124
		CAP	0.443	0.261	3.3795	58.767
		MPM	0.271	0.253	3.4095	78.458
		Proposed	**0.176**	**0.248**	**3.5073**	**79.536**
	Level-4	DCP	0.354	0.263	3.3161	66.767
		CAP	0.457	0.265	3.3736	57.458
		MPM	0.296	0.257	3.3960	75.598
		Proposed	**0.189**	**0.253**	**3.4551**	**77.325**
5	Level-3	DCP	0.337	0.252	3.0253	**68.498**
		CAP	0.468	0.255	3.1207	51.945
		MPM	0.369	0.252	3.1151	66.230
		Proposed	**0.196**	**0.246**	**3.4417**	62.743
	Level-4	DCP	0.391	0.256	2.8429	**65.644**
		CAP	0.556	0.261	3.1690	49.168
		MPM	0.440	0.258	3.0726	62.196

		Proposed	**0.228**	**0.251**	**3.3052**	59.926
10	Level-3	DCP	0.263	0.271	2.7363	**86.330**
		CAP	0.385	0.278	2.7743	63.755
		MPM	0.278	0.267	**2.8444**	83.162
		Proposed	**0.145**	**0.265**	2.8172	85.386
	Level-4	DCP	0.276	0.274	2.8540	**84.565**
		CAP	0.402	0.281	2.8672	62.315
		MPM	0.308	0.272	**2.9426**	79.911
		Proposed	**0.163**	**0.269**	2.8681	81.597
15	Level-3	DCP	0.329	0.270	3.3597	55.406
		CAP	0.508	0.278	3.1900	46.009
		MPM	0.305	0.260	3.2100	**66.943**
		Proposed	**0.197**	**0.251**	**3.3964**	58.358
	Level-4	DCP	0.347	0.282	3.1051	55.445
		CAP	0.558	0.291	2.9624	45.261
		MPM	0.356	0.276	2.9541	**62.988**
		Proposed	**0.220**	**0.266**	**3.1330**	57.523
20	Level-3	DCP	0.417	0.319	2.5731	38.031
		CAP	0.561	0.317	2.5305	37.504
		MPM	0.419	0.299	2.6118	47.585
		Proposed	**0.188**	**0.288**	**2.7140**	**55.808**
	Level-4	DCP	0.450	0.309	2.5195	37.749
		CAP	0.624	0.304	2.4998	37.508
		MPM	0.474	0.288	2.4910	46.795
		Proposed	**0.212**	**0.276**	**2.7138**	**55.012**

5. Conclusions

The proposed method of PASD-MEF is based on multi-exposure image fusion. The MEF works on the adaptive structure decomposition technique. A sequence of under-exposed images is extracted from the input single smoke and burry image. The Gamma correction is implemented to achieve a set of under-exposed images while the SLA scheme is applied for saturation adjustment. Adaptive structure decomposition (ASD) is used during the MEF procedure. The adaptive patch decomposition integrates all common regions from a series of images that have better contrast and saturation. Whereas MEF fused these sets of images into a single de-smoke image. The qualitative as well as quantitative results showed that the proposed method significantly improves the visual quality of images and also reduces the smoke from images. The main goal of this paper is to remove smoke and enhanced laparoscopic images. The improved quality of images is useful in image-guided surgery and also helpful for surgeons for better visibility during surgery.

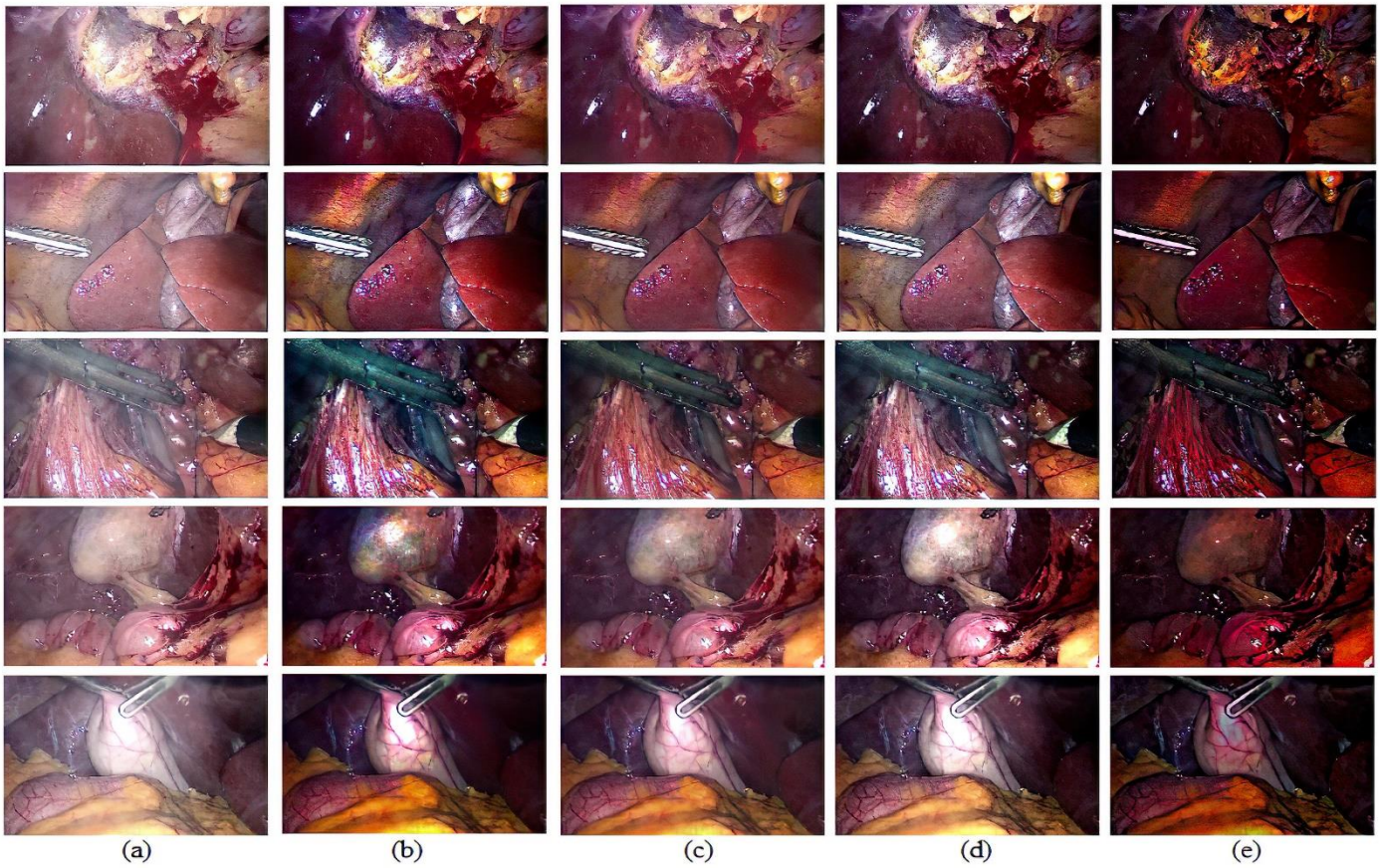

Figure 5. Qualitative visual results of smoke level 3 laparoscopic images (a) Input smoke and blur laparoscopic images where (b) ~ (e) images are resultant smoke-free and enhanced images. (b) DCP [8] (c) CAP [19] (d) MPM [34] (e) Proposed method.

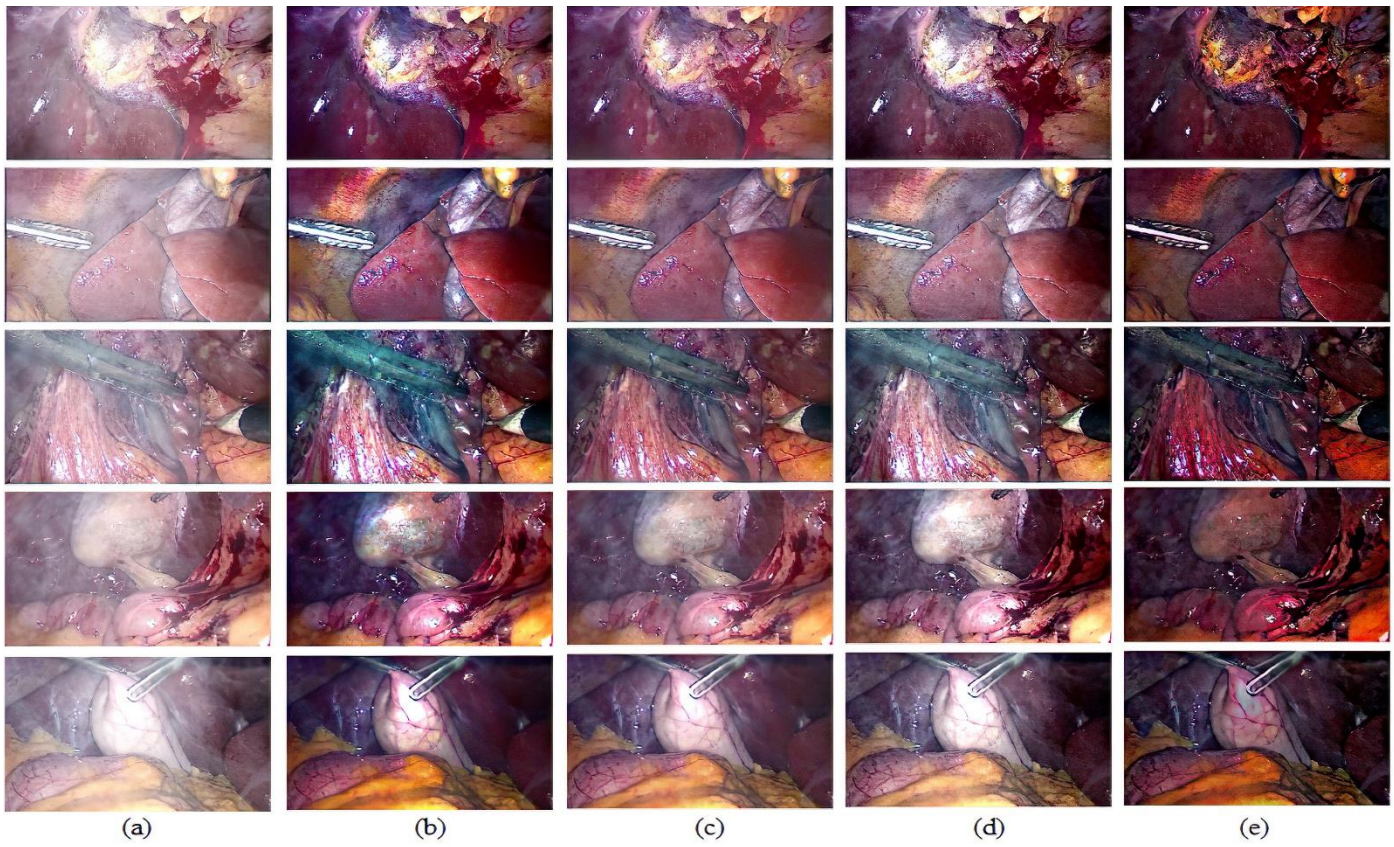

Figure 6. Qualitative visual results of smoke level 4 laparoscopic images (a) Input smoke and blur Laparoscopic images where (b) ~ (e) images are resultant smoke-free and enhanced images. (b) DCP [8] (c) CAP [19] (d) MPM [34] (e) Proposed method.

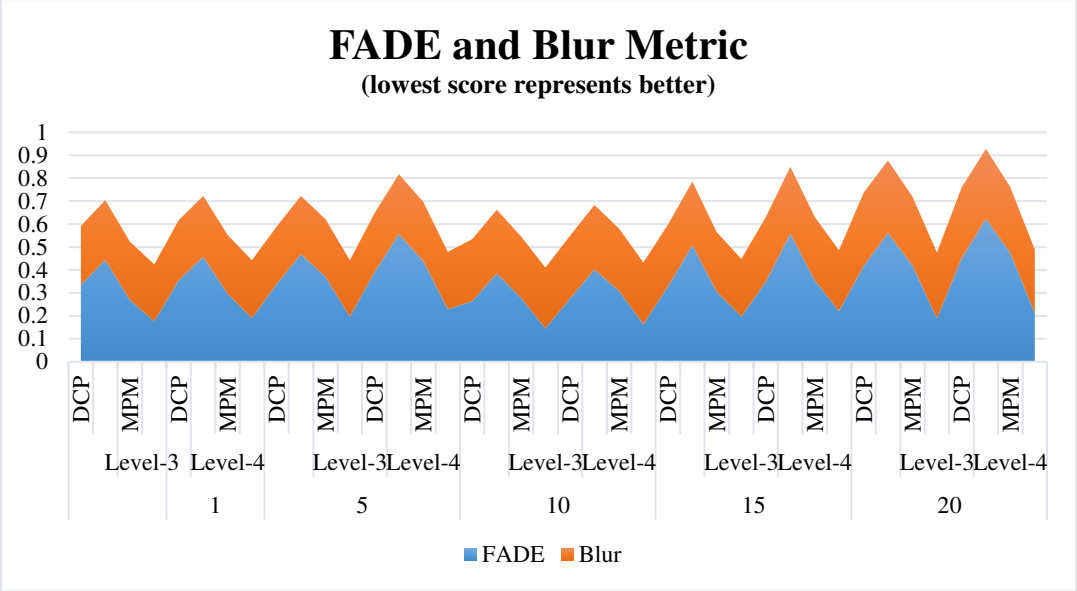

Figure 7. Graphical objective evaluation results of FADE and blur metric.

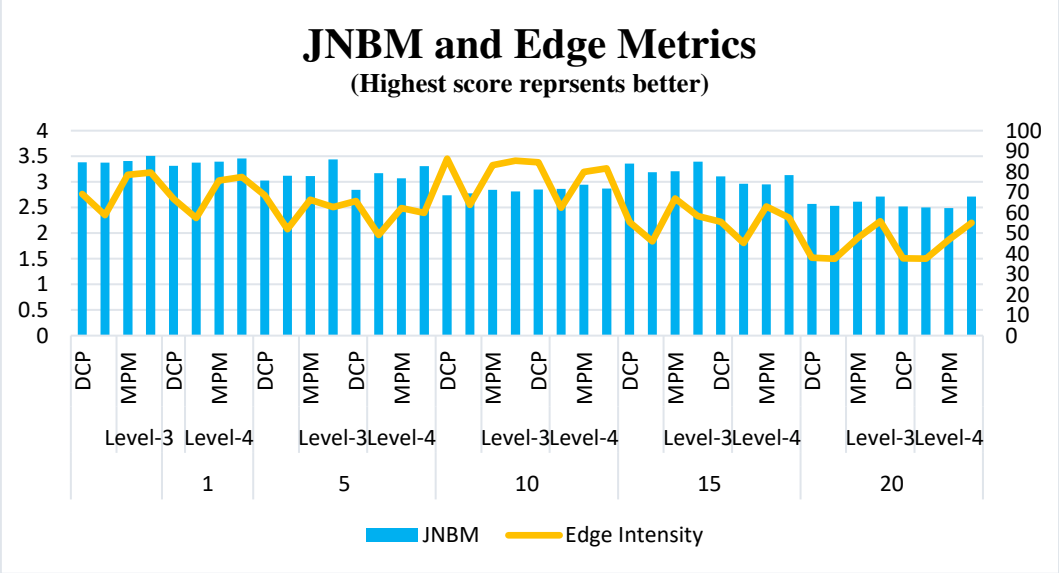

Figure 8. Graphical objective evaluation result of JNBM and Edge intensity metric.

Supplementary Materials: The following are available online at www.mdpi.com/xxx/s1, Figure S1: title, Table S1: title, Video S1: title.

Author Contributions: For research articles with several authors, a short paragraph specifying their individual contributions must be provided. The following statements should be used "Conceptualization, X.X. and Y.Y.; methodology, X.X.; software, X.X.; validation, X.X., Y.Y. and Z.Z.; formal analysis, X.X.; investigation, X.X.; resources, X.X.; data curation, X.X.; writing—original draft preparation, X.X.; writing—review and editing, X.X.; visualization, X.X.; supervision, X.X.; project administration, X.X.; funding acquisition, Y.Y. All authors have read and agreed to the published version of the manuscript." Please turn to the CRediT taxonomy for the term explanation. Authorship must be limited to those who have contributed substantially to the work reported.

Funding: This research received no external funding.

Institutional Review Board Statement: In this section, please add the Institutional Review Board Statement and approval number for studies involving humans or animals. Please note that the Editorial Office might ask you for further information. Please add "The study was conducted according to the guidelines of the Declaration of Helsinki, and approved by the Institutional Review Board (or Ethics Committee) of NAME OF INSTITUTE (protocol code XXX and date of approval)." OR "Ethical review and approval were waived for this study, due to REASON (please provide a detailed justification)." OR "Not applicable." for studies not involving humans or animals. You might also choose to exclude this statement if the study did not involve humans or animals.

Informed Consent Statement: Any research article describing a study involving humans should contain this statement. Please add "Informed consent was obtained from all subjects involved in the study." OR "Patient consent was waived due to REASON (please provide a detailed justification)." OR "Not applicable." for studies not involving humans. You might also choose to exclude this statement if the study did not involve humans.

Written informed consent for publication must be obtained from participating patients who can be identified (including by the patients themselves). Please state "Written informed consent has been obtained from the patient(s) to publish this paper" if applicable.

Data Availability Statement: In this section, please provide details regarding where data supporting reported results can be found, including links to publicly archived datasets analyzed or generated during the study. Please refer to suggested Data Availability Statements in section "MDPI Research Data Policies" at https://www.mdpi.com/ethics. You might choose to exclude this statement if the study did not report any data.

Acknowledgments: In this section, you can acknowledge any support given which is not covered by the author contribution or funding sections. This may include administrative and technical support, or donations in kind (e.g., materials used for experiments).

Conflicts of Interest: The authors declare no conflict of interest.

References

1. D. A. S. Toyanov, "Surgical Vision," Ann. Biomed. Eng., vol. 40, no. 2, pp. 332–345, 2012.
2. K. Y. Hahn and D. W. Kang, "Removal of Hazardous Surgical Smoke Using a Built-in-Filter Trocar : A Study in Laparoscopic Rectal Resection," Surg. Laparosc. Endosc. Percutan. Tech., vol. 27, no. 4, pp. 341–345, 2017.
3. H. Alberto-moreno, J. Ortiz-echeverri, and G. Flores, "Desmoking laparoscopy surgery images using an image-to-image translation guided by an embedded dark channel," arXiv Prepr. arXiv, pp. 1–9, 2020.
4. B. Sdiri, A. Beghdadi, F. A. Cheikh, M. Pedersen, and O. J. Elle, "An adaptive contrast enhancement method for stereo endoscopic images combining binocular just noticeable difference model and depth information," Electron. Imaging, vol. 13, no. 2016, pp. 1–7, 2016.
5. X. Luo, A. J. Mcleod, S. Member, S. E. Pautler, C. M. Schlachta, and T. M. Peters, "Vision-Based Surgical Field Defogging," IEEE Trans. Med. Imaging, vol. 0062, no. MARCH, pp. 1–10, 2017.
6. A. Baid, A. Kotwal, R. Bhalodia, S. N. Merchant, and S. P. Awate, "JOINT DESMOKING, SPECULARITY REMOVAL, AND DENOISING OF LAPAROSCOPY IMAGES VIA GRAPHICAL MODELS AND BAYESIAN INFERENCE Indian Institute of Technology (IIT) Bombay. University of Utah.," in IEEE 14th International Symposium on Biomedical Imaging, 2017, pp. 732–736.
7. A. Kotwal, "JOINT DESMOKING AND DENOISING OF LAPAROSCOPY IMAGES Department of Electrical Engineering Indian Institute of Technology (IIT) Bombay Department of Computer Science and Engineering Indian Institute of Technology (IIT) Bombay," in IEEE 13th International Symposium on Biomedical Imaging (ISBI), 2016, pp. 1050–1054.
8. K. He, J. Sun, and X. Tang, "Single Image Haze Removal Using Dark Channel Prior," IEEE Trans. Pattern Anal. Mach. Intell., vol. 33, no. 12, pp. 2341–2353, 2011.
9. R. T. Tan, "Visibility in Bad Weather from a Single Image," in IEEE Conference on Computer Vision and Pattern Recognition, 2008, pp. 1–8.
10. A. Galdran, "AC PT US CR," Signal Processing, 2018.
11. Y. Li, Q. Miao, R. Liu, J. Song, Y. Quan, and Y. Huang, "Neurocomputing A multi-scale fusion scheme based on haze-relevant features for single image dehazing," Neurocomputing, vol. 283, pp. 73–86, 2018.
12. Z. Rahman, D. J. Jobson, G. A. Woodell, and C. Science, "Retinex Processing for Automatic Image Enhancement," in Human Vision and Electronic Imaging VII, 2004, pp. 390–401.
13. C. O. Ancuti and C. Ancuti, "Single Image Dehazing by Multi-Scale Fusion," IEEE Trans. Image Process., vol. 22, no. 8, pp. 3271–3282, 2013.
14. G. Thomas, D. Flores-tapia, and S. Pistorius, "Histogram Specification : A Fast and Flexible Method to Process Digital Images," IEEE Trans. Instrum. Meas. •, vol. 609(5), no. January 2014, pp. 1565–1578, 2011.

15. Z. Yu, "A Fast And Adaptive Method For Image Contrast Enhancement," in International Conference on Image Processing, 2004, 2015, no. September, pp. 1001–1004.
16. Z. Rong and W. L. Jun, "Improved wavelet transform algorithm for single image dehazing," Opt. - Int. J. Light Electron Opt., vol. 125, no. 13, pp. 2013–2015, 2014.
17. S. Member, S. Member, and S. Member, "Robust Multi-Exposure Image Fusion : A Structural Patch Decomposition Approach," IEEE Trans. Image Process., vol. 26, no. 5, pp. 2519–2532, 2017.
18. J. Tarel and N. Hauti, "Fast Visibility Restoration from a Single Color or Gray Level Image," in IEEE 12th International Conference on Computer Vision, 2009, pp. 2201–2208.
19. Q. Zhu, J. Mai, L. Shao, and S. Member, "A Fast Single Image Haze Removal Algorithm Using Color Attenuation Prior," IEEE Trans. Image Process., vol. 24, no. 11, pp. 3522–3533, 2015.
20. A. G. B, J. Vazquez-corral, D. Pardo, and M. Bertalm, "A Variational Framework for Single Image Dehazing," in InEuropean Conference on Computer Vision, 2015, vol. 1, pp. 259–270.
21. Y. Li, Y. Sun, M. Zheng, X. Huang, and G. Qi, "A Novel Multi-Exposure Image Fusion Method Based on Adaptive Patch Structure," ENTROPY, vol. 20, no. 12, pp. 1–17, 2018.
22. Y. Liu, X. Chen, R. K. Ward, and Z. J. Wang, "Medical image fusion via convolutional sparsity based morphological component analysis," IEEE Signal Process. Lett., vol. 26, no. 3, pp. 485–489, 2019.
23. I. Fusion, "A Novel Geometric Dictionary Construction Approach for Sparse Representation Based Image Fusion," Entropy, vol. 19, no. 7, pp. 1–17, 2017.
24. Z. Zhu, H. Yin, Y. Chai, Y. Li, and G. Qi, "A novel multi-modality image fusion method based on image decomposition and sparse representation," Inf. Sci. (Ny)., vol. 432, pp. 516–529, 2018.
25. Z. Zhu, Y. Chai, H. Yin, and Y. Li, "Author ' s Accepted Manuscript modality medical image fusion Reference : To appear in : Neurocomputing," Neurocomputing, vol. 214, pp. 471–482, 2016.
26. K. He, J. Sun, and X. Tang, "LNCS 6311 - Guided Image Filtering," Eur. Conf. Comput. Vision, vol. 6311, pp. 1–14, 2010.
27. H. Li, Y. Wang, Z. Yang, R. Wang, X. Li, and D. Tao, "Discriminative dictionary learning-based multiple component decomposition for detail-preserving noisy image fusion," IEEE Trans. Instrum. Meas., vol. 69, no. 4, pp. 1082–1102, 2019.
28. H. Li, X. He, D. Tao, Y. Tang, and R. Wang, "Joint medical image fusion , denoising and enhancement via discriminative low-rank sparse dictionaries learning," Pattern Recognit., vol. 79, pp. 130–146, 2018.
29. H. Li, H. Qiu, Z. Yu, and Y. Zhang, "Infrared Physics & Technology Infrared and visible image fusion scheme based on NSCT and low-level visual features," INFRARED Phys. Technol., vol. 76, pp. 174–184, 2016.
30. F. U. Jin and J. Sim, "A Novel Image Fusion Framework Based on Sparse Representation and Pulse Coupled Neural Network," IEEE Access, vol. 7, pp. 98290–98305, 2019.
31. G. Qi, L. Chang, Y. Luo, Y. Chen, Z. Zhu, and S. Wang, "A Precise Multi-Exposure Image Fusion Method Based on Low-level Features," sensors Artic., vol. 20, no. 6, pp. 1–18, 2020.
32. B. L. T. Characterization, S. Ono, S. Member, and T. Miyata, "Cartoon-Texture Image Decomposition Using," vol. 23, no. 3, pp. 1128–1142, 2014.
33. L. A. Vese and S. J. Osher, "Modeling Textures with Total Variation Minimization and Oscillating Patterns in Image Processing," J. ofScientific Comput., vol. 19, no. December, pp. 553–572, 2003.
34. R.-A. J. Salazar-Colores S, Cruz-Aceves I, "Single image dehazing using a multilayer perceptron," J. Electron. Imaging, vol. 27(4), p. 043022, 2018.
35. A. P. Twinanda, S. Shehata, D. Mutter, J. Marescaux, M. De Mathelin, and N. Padoy, "EndoNet : A Deep Architecture for Recognition Tasks on Laparoscopic Videos," pp. 1–11.
36. Z. Amjad, A. Beghdadi, F. Alaya, and M. Kaaniche, "Towards a Video Quality Assessment based Framework for Enhancement of Laparoscopic Videos."
37. "'Image & video quality assessment at live,.'" [Online]. Available: https://live.ece.utexas.edu/research/fog/. [Accessed: 29-Aug-2020].
38. L. K. Choi, J. You, and A. C. Bovik, "Referenceless Prediction of Perceptual Fog Density and Perceptual Image Defogging," IEEE Trans. IMAGE Process., vol. 24, no. 11, pp. 3888–3901, 2015.
39. R. Ferzli and L. J. Karam, "A NO-REFERENCE OBJECTIVE IMAGE SHARPNESS METRIC BASED ON JUST-NOTICEABLE BLUR AND PROBABILITY SUMMATION," in IEEE International Conference on Image Processing, 2007, pp. 445–448.
40. R. Ferzli, L. J. Karam, and S. Member, "A No-Reference Objective Image Sharpness Metric Based on the Notion of Just Noticeable Blur (JNB)," IEEE Trans. Image Process., vol. 18, no. 4, pp. 717–728, 2009.
41. N. I. H. Autière, J. E. A. N. H. T. Arel, D. I. A. Ubert, and É. R. I. C. D. Umont, "BLIND CONTRAST ENHANCEMENT ASSESSMENT BY GRADIENT RATIOING AT VISIBLE EDGES," Image Anal Stereol 2008;2787-95, vol. 27, no. 1, pp. 87–95, 2008.
42. P. Ladret and M. Nicolas, "The Blur Effect : Perception and Estimation with a New No-Reference Perceptual the Blur Effect : Perception and Estimation with a New No-Reference Perceptual Blur Metric," Hum. Vis. Electron. Imaging XII, vol. 6492, no. September 2014, p. 64920I, 2007.